Supplement

A founder mutation in EHD1 presents with tubular proteinuria and deafness

Naomi Issler [1#], Sara Afonso [2#], Irith Weissman [3#], Katrin Jordan [2], Alberto Cebrian-Serrano [4], Katrin Meindl [2], Eileen Dahlke [5], Konstantin Tziridis [6], Guanhua Yan [7], José M. Robles-López [7], Lydia Tabernero [7], Vaksha Patel [1], Anne Kesselheim [1], Enriko D. Klootwijk [1], Horia C. Stanescu [1], Simona Dumitriu [1], Daniela Iancu [1], Mehmet Tekman [1], Monika Mozere [1], Graciana Jaureguiberry [1], Priya Outtandy [1], Claire Russell [7], Anna-Lena Forst [2], Christina Sterner [2], Elena-Sofia Heinl [2], Helga Othmen [2], Ines Tegtmeier [2], Markus Reichold [2], Ina Maria Schiessl [9], Katharina Limm [10], Peter Oefner [10], Ralph Witzgall [11], Lifei Fu [12], Franziska Theilig [5], Achim Schilling [6], Efrat Shuster Biton [3], Limor Kalfon [3], Ayalla Fedida [3], Elite Arnon-Sheleg [3], Ofer Ben Izhak [13], Daniella Magen [13], Yair Anikster [14], Holger Schulze [6], Christine Ziegler [12], Martin Lowe [7], Benjamin Davies [4], Detlef Böckenhauer [1], Robert Kleta [1*#], Tzipora C. Falik Zaccai [3#], Richard Warth [2*#]

# contributed equally

[1] Department of Renal Medicine, UCL, London, UK
[2] Medical Cell Biology, University Regensburg, Germany
[3] Galilee Medical Center, Nahariya, Israel
[4] Wellcome Centre Human Genetics, University Oxford, UK
[5] Institute of Anatomy, University Kiel, Germany
[6] ENT Clinic, University Hospital Erlangen, Germany
[7] Division of Molecular & Cellular Function, University Manchester, UK
[8] Royal Veterinary College, London, UK
[9] Institute of Physiology, University Regensburg, Germany
[10] Institute of Functional Genomics, University Regensburg, Germany
[11] Molecular and Cellular Anatomy, University Regensburg, Germany
[12] Structural Biology, University Regensburg, Germany
[13] Pediatric Nephrology Institute, Haifa, Israel
[14] Sheba Medical Center, Tel-Aviv, Israel

*Corresponding authors:

Robert Kleta, MD/PhD
Potter Chair of Nephrology
Department of Renal Medicine
University College London
Rowland Hill Street, London NW3 2PF, UK
phone: ++44-20 7314 7554
email: r.kleta@ucl.ac.uk

Richard Warth, MD
Medical Cell Biology
University Regensburg
Universitaetsstr. 31, 93053 Regensburg, Germany
phone: ++49 941 943 2894
email: richard.warth@ur.de

Contents

Supplemental Methods

Ehd1 knockout mice

Experiments were performed according to the guidelines for the care and use of laboratory animals published by the US National Institutes of Health and were approved by the local councils for animal care according to the German law for animal care. Animal experiments on mice to assess renal function were approved by the Regierung Unterfranken, Germany.

We thank the Wellcome Trust Sanger Institute Mouse Genetics Project (Sanger MGP) and its funders for providing the mutant mouse line C57BL/6NTac-Ehd1$^{tm1a(EUCOMM)Wtsi/WtsiBiat}$ (https://www.mousephenotype.org/data/alleles/MGI:1341878/tm1a(EUCOMM)Wtsi), and the European Mouse Mutant Archive (https://www.infrafrontier.eu; EMMA ID: EM:05712) from which the mouse line was received. These mice carrying a floxed exon 2 of *Ehd1* were bred with a global 129/Sv Cre Recombinase pCX-NLS Cre mouse. In the offspring deletion of exon 2 was confirmed and mice were crossed to obtain homozygous progeny for the *Ehd1* gene deletion (*Ehd1*$^{-/-}$).

Ehd1$^{R398W/R398W}$ knockin mice

The *Ehd1* knockin mice were generated in house (Wellcome Centre for Human Genetics, University of Oxford, United Kingdom) using Crispr/Cas9 technologies. A CRISPR/Cas9 nuclease was designed against the sequence 5'-GATGGTGATGGTGCGCCAGG-'3 within exon 5 (ENSMUSE00000232103) of the mouse *Ehd1* gene, the target site of which encompasses the Arginine-398 residue which we identified to be mutated to a Tryptophan residue in families with hereditary tubular proteinuria and hearing deficit. A single stranded oligonucleotide harboring the desired point mutation was designed and used as a template for homology directed repair to introduce the orthologous mutation into the mouse genome. The single-strand oligodeoxynucleotide (ssODN) and the guide-RNA, prepared by in vitro transcription, for the designed CRISPR/Cas9 nuclease were microinjected into fertilized C57BL/6J oocytes prepared from transgenic female mice that overexpress Cas9 [1]. In the resulting litters, multiple founder mice were generated which harbored the desired R398W mutation. The production of the knockin mice was carried out in accordance with UK Home Office Animal [Scientific Procedures] Act 1986, with procedures reviewed by the Clinical Medicine Animal Welfare and Ethical Review Board at the University of Oxford, and conducted under project license PPL 30/3085.

Immunostaining

Mice were sacrificed by exsanguination in deep anesthesia (2.5% isoflurane). Immediately post mortem, the animals were perfused via the abdominal aorta with 3% paraformaldehyde dissolved in a solution of 100 mM sucrose, 90 mM NaCl, 15 mM K_2HPO_4, 1 mM EGTA and 2 mM $MgCl_2$ (pH 7.4). The fixed kidneys were removed and either frozen in liquid nitrogen for cryo-sectioning or further processed for standard paraffin embedding.

For immunofluorescence staining on paraffin-embedded tissue, the sections were deparaffinized and epitope unmasking was performed by incubation in citrate buffer (pH 6.0) at 95°C for 15 min. On cryo-sections epitope unmasking was performed by incubation in 0.1% SDS solution for 5 min. Unspecific

antibody binding sites were blocked using 5% BSA solution for 10 min. Primary and secondary antibodies were diluted in PBS based solution containing 0.5% BSA and 0.04% Triton X-100. Primary antibody incubation was performed overnight at 4°C. Tissue sections were washed with PBS before adding the secondary antibody for 1 h at room temperature. Sections were mounted using DAKO glycergel mounting medium (Agilent). Immunofluorescence signals of stained sections were analyzed using an inverted microscope (Axiovert 200, Zeiss) or a confocal microscope (LSM 710, Zeiss).

Stimulated-Emission–Depletion (STED) super-resolution microscopy

For STED microscopy, Cryosections for Rab11A staining were antigen retrieved using 0.5% tritonX-100 in PBS. Paraffin sections were used for triple-antibody staining of EHD1/Cubilin/Megalin. Heat-induced antigen retrieval were performed in citrate buffer (pH 6). Sections were blocked with 10% donkey serum/PBS and sequentially incubated with primary antibodies in 5% donkey serum/PBS overnight. Suitable StarRed-, Star580-, Alexa488-coupled secondary antibodies (Abberior, Göttingen, Germany; Dianova, Hamburg, Germany) were used. Counter staining were performed using Acti-stain 488 Phalloidin (Cytoskeleton) and/or 4',6-diamidino-2-phenylindole. Sections were mounted with Abberior Liquid Mount and analyzed using a multilaser confocal scanning microscope and/or stimulated-emission-depletion super-resolution microscopy (see below).

Images were acquired using Facility Line (Abberior Instruments, Göttingen, Germany) with Olympus IX83 microscope (Germany) and Imspector software (Abberior Instruments) in confocal microscopy mode or STED mode. The images were de-convolved using Huygens Professional Software (version 20.10, Scientific Volume Imaging B.V., Netherlands). The Classic Maximum Likelihood Estimation (CMLE) algorithm for deconvolution was performed using standard setting (quality change threshold 0.1%).

Antibody/substance	Type	Dilution for immuno-fluorescence	Producer
anti-ARL13B, rabbit polyclonal IgG	Prim.-Ab	1:500	Proteintech Germany, St. Leon-Rot, Germany
anti-EHD1, rabbit monoclonal [EPR4954] IgG	Prim.-Ab	1:200	Abcam, Cambridge, UK
anti-EHD1 for Supplemental Figure 12	Prim.-Ab	1:200	Kind gift from S. Caplan, University of Nebraska
Anti-Aquaporin-2 (C17), goat polyclonal antibody	Prim.-Ab	1:500	Santa Cruz, Heidelberg, Germany
Anti-Megalin, guinea pig polyclonal antibody	Prim.-Ab	1:1000	F. Theilig, University of Kiel [2]
Anti-MICAL-L1, guinea pig polyclonal antibody, H00085377 B01P	Prim.-Ab	1:200	Abnova
anti-Rab11A, rabbit polyclonal antibody	Prim.-Ab	1:100	Invitrogen
anti-Cubilin (T-16), goat polyclonal antibody	Prim.-Ab	1:30	Santa Cruz
anti-Arf6, mouse monoclonal	Prim.-Ab	1:100	Kind gift from J. Barhanin [3]
anti-acetylated tubulin, mouse monoclonal, (T6793)	Prim.-Ab	1:100	Sigma Aldrich

StarRED donkey anti-rabbit	Sec.-Ab	1:50	Abberior; Dianova, Hamburg, Germany
Star580 donkey anti-rabbit	Sec.-Ab	1:50	Abberior; Dianova, Hamburg, Germany
Star580 donkey anti-mouse	Sec.-Ab	1:50	Abberior; Dianova, Hamburg, Germany
Alexa Fluor® 488 donkey anti-goat	Sec.-Ab	1:50	Dianova, Hamburg, Germany
Acti-stain 488 Phalloidin	Actin Stain	1:200	Cytoskeleton, Denver, USA
Alexa Fluor® 488 donkey anti-rabbit	Sec.-Ab	1:400	Thermo Fisher Scientific, Dreieich, Germany
Alexa Fluor® 555 donkey anti-rabbit	Sec.-Ab	1:400	Thermo Fisher Scientific, Dreieich, Germany
Alexa Fluor® 555 donkey anti-goat	Sec.-Ab	1:400	Invitrogen, Karlsruhe, Germany
Alexa Fluor® 647 donkey anti-guinea-pig	Sec.-Ab	1:400	Invitrogen, Karlsruhe, Germany
HOE33342 ($5x10^{-2}$ M)	Nuclear stain	1:400	Invitrogen, Karlsruhe, Germany
DAPI	Nuclear stain	1:2000	Thermo Fischer

Fluorescent labeling of β_2-microglobulin

1 mg protein of recombinant, human β_2-microglobulin expressed in *E. coli* (Merck) was used for conjugation with the fluorescent tag Alexa Fluor™ 546 using the Alexa Fluor™ 546 Protein Labelling Kit (Thermo Fisher) according to the manufacturer's instructions. The conjugates were separated from the unconjugated dye by exclusion purification resin. The obtained β_2-microglobulin-Alexa Fluor 546 conjugate had a concentration of ~750 µM.

Reabsorption of β_2-microglobulin

To assess renal reabsorption of β_2-microglobulin, age-matched mice were anesthetized using isoflurane inhalation (1.5% isoflurane in a gas mixture of 50% oxygen and 50% nitrogen). A catheter was placed into the femoral vein, the bladder was emptied and a 1:50 dilution (in 0.9% NaCl) of the above-mentioned Alexa Fluor 546 labeled β_2-microglobulin was injected into the femoral vein at a dose of 20 µl/g body weight. 30 min later, urine and blood were collected and the mice were sacrificed by exsanguination via the vena cava. Immediately post mortem, animals were perfused with fixative via the abdominal aorta. Both kidneys were harvested; one was homogenized in distilled water, the other one was prepared for cryo-sectioning. The fluorescence intensity of Alexa Fluor 546 in plasma, urine and kidney homogenate was measured using a microplate reader (NOVOstar microplate reader).

RNAScope of kidneys

RNAScope experiments were performed on paraffin-embedded kidneys using the *RNAScope® 2.5 HD Assay* Kit (ACD) according to the manufacturer's instructions.

Auditory brainstem response measurement

Animals aged between 6-8 weeks were used for the measurement of the auditory brainstem response. Mice were anaesthetized using a mixture of ketamine (96 mg/kg), xylazine (4 mg/kg) and physiological NaCl solution at a mixing ratio of 9:1:8, initial dose: 0,3 mL s.c.. Mice were placed within a sound-attenuated chamber on a thermally controlled heating pad at 37°C, and frequency-specific auditory brainstem responses (f-ABR) were measured. The protocol was performed as previously described [4]. Briefly, f-ABR were measured via subcutaneously placed thin silver wire electrodes (0.25 mm diameter) using a low noise amplifier (JHM NeuroAmp 401, J. Helbig Messtechnik, Mainaschaff, Germany; amplification 10,000; bandpass filter 400 to 2,000 Hz and 50 Hz notch filter) in combination with a custom-made Python program (Python 2.6) for stimulation and data recording. Auditory stimuli of 4, 8, 16 and 32 kHz were presented free-field to one ear at 3 cm distance from the animal's pinna via a custom-made speaker. The speaker's frequency response function was corrected to be flat within ±1 dB. Stimuli presented were pure tones (6 ms duration including 2 ms cosine-squared rise and fall times) between the range of 1 and 32 kHz. 300 stimuli were presented with alternating inverted phase with a repetition rate of 4 Hz. The stimuli of all tested frequencies were presented pseudorandomized with different sound pressure levels between 30 dB and 100 dB with a step width of 5 dB. To obtain the f-ABR-based hearing thresholds, the mean sound intensity dependent f-ABR wave root-mean-square values independent for each frequency were fitted by hard-sigmoid functions. Thresholds were defined automatically by a custom-made Python program at the inflection point of that hard sigmoid fit. Variance of the calculated ABR thresholds were obtained by data subsampling. Data were discarded at frequencies where this procedure was not possible, for example, at very low signal-to-noise ratios. The statistical analysis of the individual and group threshold data was performed in Origin.

Intravital microscopy of renal proximal tubular endocytosis

Mice were anesthetized through inhalation of isoflurane (1.5-2.5% isoflurane). The body temperature was maintained at 37°C by placing the animals on an operating table with a servo-controlled heating plate. A cannula connected to a syringe was inserted into the right jugular for the intravenous infusion of the dyes. For kidney imaging, the left kidney was exposed by making a small flank incision. The experiments were performed using a Zeiss LSM 710 confocal fluorescence microscope. Excitation was achieved using a Chameleon Ultra-II MP laser (Coherent Deutschland, Dieburg, Germany) at 940 nm with a laser power of 20% of 3200 mW. Eight-bit 1454 x 1454 pixel images (providing a theoretical dynamic range for intensities measurements of 0–65536 pixel intensity) were obtained using a pixel dwell time of 3.15 µs and a line average of one by applying a 40x long distance (LD) C- Apochromat 40/1.1 water objective. The emissions were collected using external detectors: Nondescanned detectors with filter set 1 (green channel): beam splitter 500–550 and long pass (LP) 555 and filter set 2 (red channel): beam splitter P 565–610 including mirror. The detector settings were kept constant for all measurements: for the green and red channels, respectively, the master gain was 600/600, the digital gain was 10/10, and the offset was -0.0/0.0. To label the vasculature, a 25 mg/ml solution of FITC-500 kDa Dextran conjugate dissolved in PBS was first concentrated using Nanosep Centrifugal (VWR International, Darmstadt, Germany) and injected intravenously (0.37 µl/g body weight). The

fluorescence was detected using the green channel. After 1 min, the Alexa Fluor 546-labeled β_2-microglobulin dissolved in PBS was injected intravenously (1.56 µl/g body weight) and the proximal tubular β_2-microglobulin uptake was measured as the increase in the tubular fluorescence intensity during the 30 min after injection. The fluorescence was detected using the red channel. The mean fluorescence intensity of Alexa Fluor 546-labeled β_2-microglobulin measured in 3–6 proximal tubules per animal over time (30 min, 15 images) and the background readings for the proximal tubular autofluorescence before labeled β_2-microglobulin injection were assessed using ImageJ V1.37c. The reabsorption capacity of the proximal tubules was compared after 2, 4, 10, 20 and 30 min of β_2-microglobulin injection by assessing the mean fluorescence intensity of β_2-microglobulin per tubule and subtracting the background fluorescence.

Zebrafish strains and husbandry

Zebrafish were raised and maintained at the University of Manchester Biological Services Unit according to the UK Animals Act 1986. The wildtype line was of the AB background.

Zebrafish RNA isolation, RT-PCR and Q-PCR

Total RNA was isolated from zebrafish embryos using Trizol (Invitrogen) and reverse-transcribed with Superscript First Strand (Invitrogen) to produce cDNA. For direct visualization of amplification products, cDNA was amplified using standard PCR conditions and appropriate primer pairs. Q-PCR was performed using SYBR Green (Sigma-Aldrich) according to the manufacturer's protocol. 0.5 µl cDNA template from a 20 µl aliquot generated from 5 µg of RNA was used per reaction. Each experiment was run in duplicate and was repeated on three individually obtained RNA extracts. Studies were performed using the ABI PRISM 7000 sequence detector system (Applied Biosystems Ltd).

Morpholino injections into zebrafish

Morpholinos were obtained from GeneTools. The standard control morpholino had the sequence CCTCTTACCTCAGTTACAATTTATA (https://www.gene-tools.com/content/negative-control-morpholino-oligos). Morpholinos targeting zebrafish *ehd1* were the same as described previously, with the following sequences: *ehd1a* (CTGAACATGGTGGACGTTACACGAC); *ehd1b* (ATCTTTGTTAGACCAACTGAACATT) and were injected with morpholino targeting p53 (1 nl of a 250 µM stock) into one cell stage embryos as described previously [5, 6].

Injection and analysis of endocytic tracer

Lysine-fixable 10 kDa dextran labelled with Alexa 488 (Molecular Probes) was prepared in PBS at 2 µg/µl final concentration, and 1 nl was injected into the larval circulatory system. Zebrafish larvae at 4 dpf were anesthetized with 0.2 mg/ml MS222 (Sigma) in chorion water, and tracer injected into the common cardinal vein using a glass micropipette PLI-90 Pico-Injector (Harvard Apparatus). Pronephric uptake was assessed at 2.5 h on whole mounts using a fluorescence dissecting stereomicroscope (Leica MZ10F). Statistical analysis was performed using the Pearson' s chi-squared test with Prism software (Prism Software Corporation).

Western blotting of zebrafish larvae

Larvae were culled by anaesthetic overdose and 100 collected per condition in 1.5 mL Eppendorf tubes. Embryos were then triturated ~15 times in Ginzburg fish ringers' solution (110 mM NaCl, 3.5 mM KCl, 2.7 mM $CaCl_2 \cdot 2H_2O$, 10 mM Tris pH 8.5) containing 0.75 mM EDTA, 0.3 mM PMSF, and 20x protease inhibitor cocktail to remove the yolk sac. Larvae were centrifuged at 1800 rpm for 1 min, supernatant removed, and washed again in Ginzburg solution before analysis by Western blotting with antibodies to EHD1 (Steve Caplan, University of Nebraska) and GAPDH (Santa Cruz SC-25778).

Ethics statement on Zebrafish experiments

All work was performed under the UK Home Office animal project license number 70/9091. Local animal care was provided by the University of Manchester BSF Unit. Zebrafish larvae at 4 dpf were anesthetized with 0.2 mg/ml MS222 for injection of endocytic tracer. Following the experiment, euthanasia was performed by incubation in 0.2 mg/ml MS222 for >2h.

Proteomics

Mouse kidney was transferred to 2-ml Precellys tubes (Precellys® Keramik-Kit 1.4/2.8 mm, Bertin). Homogenisation was performed twice at 6,500 rpm for 20 sec in 1 ml of ice cold 80% MeOH by means of the Precellys® 24 Homogenisator (Bertin). Samples were then incubated at -20 °C overnight prior to centrifugation at 20,000 x g for 15 min at 4°C. Supernatant was discarded and the pellets were air-dried. Further lysis was performed in 1 ml of gel-aided sample preparation (GASP)-buffer [7] supplemented with 20 mM DTT. Total protein amount was determined using the SERVA Purple Protein Quantification Assay (SERVA Electrophoresis GmbH) according to the manufacturer's instructions. Fifty micrograms of protein lysate were then processed using the GASP protocol as described previously [7]. After tryptic digestion, the peptide extracts were redissolved in 25 µl of 5% formic acid.

Microliquid chromatographic (microLC) separations of tryptic digests were performed on an Eksigent-LC 425 (AB Sciex) coupled to an AB Sciex TripleTOF 5600+ mass spectrometer [8]. The tryptic digests (5 µg each) were injected directly onto a 150 × 0.3 mm I.D. CSH-C18 column (particle size 1.7 µm, 120 Å, Waters) and peptides were separated at a column temperature of 40 °C using a 85-min linear acetonitrile gradient (3–40%) in 0.1% formic acid atflow-rate of 6 µL/min. Samples were injected once each for mass spectrometric (MS) analysis in data-dependent acquisition (DDA) mode and Sequential Window Acquisition of all THeoretical fragment-ion spectra (SWATH), respectively [9]. For peptide library generation, the TripleTOF 5600+ mass spectrometer (AB Sciex, Darmstadt, Germany) was operated in DDA mode from 400–1,000 m/z for 250 ms, followed by acquisition of MS/MS-spectra from 230–1,500 m/z of the 20 most intensive precursor ions for 50 ms per precursor. The data were searched using ProteinPilot 5.0 (AB Sciex) against the UniProtKB/Swiss-Prot (Version 03-2021) database. For SWATH-MS, an initial 50 ms TOF-MS full scan was employed, before the entire m/z range of 230–1,500 was covered using 60 SWATH variable windows of 50 ms each [10]. For quantification of the proteins from the SWATH runs the PeakView 2.2 software (AB Sciex) and the MicroApp 2.0.1 were used.

Homology modelling of EHD1 and EHD1^{R398W}

Human EHD isoforms EHD1, EHD2 and EHD4 exhibit high sequence identities of about 70% (Supplemental Figure 7). Two homology models of EHD1 were generated based on crystal structures of the autoinhibited state of EHD2 (pdb entry code 4CDI) (Supplemental Figure 8A and 8B) and the activated state of EHD4 (pdb entry code 5MTV) (Supplemental Figure 8C and 8D) as respective templates. Arg398 in both models is located at the very end of helix α12 in front of the linker loop to the EH-domains pointing away from the dimer interface and the GTPase domain (Supplemental Figure 8B and 8D). At a first glance, a functional role for Arg398 and the phenotype seen in EHD1^{R398W} is not obvious from the homology models. However, looking into the activation mechanisms of EHD proteins points towards a problem in oligomerization as consequence of the R398W mutation found in our patients.

The auto-inhibited state differs from activated state in EHDs in the orientation of helix α8, which rotates over 60˚ around a hinge point at Pro286 (Supplemental Figure 7, black star and Supplemental Figure 8). In the inhibited state, α8 is wedged between the N-terminal helical domain α(1a,b) and a bundle of three small helices α9 - α11 (pink in Supplemental Figure 8B and 8D) which are known to be involved in membrane interactions. Activation is suggested to start with a conformational change of the N-terminal domain at the membrane surface, thereby releasing α8, which snaps like a Swiss army knife into the extended conformation (Supplemental Figure 8C and 8D). This rigid-body movement is accompanied by several changes such as the detachment of the EH-domain from the GTPase domain, re-arrangement of the membrane interacting bundle α9 - α11 (Supplemental Figure 8B and 8D), and re-folding and relocation of the KPF loop. None of these conformational changes seem to involve Arg398, which rather faces away from the KPF loop within a monomer. However, in the active state EHD1 dimers oligomerize in a front-to-back orientation mediated by the KPF loop of individual dimers (Supplemental Figure 9A and 9B). In the context of this oligomerization Arg398 in EHD1 might provide a re-enforcement of dimer-dimer interaction. A likely partner candidate is Glu106 that is located just in front of the KPF loop of the adjacent dimer. A Glu106-Arg398 interaction (Supplemental Figure 9B) might help sculpturing the oligomerization interface further.

Ab initio mutation against tryptophan in the homology model of EHD1^{R398W} did not alter the overall conformation of the EHD1 dimer but the introduction of a bulky and hydrophobic residue like tryptophan would affect this most relevant oligomerization interface (Supplemental Figure 9C). In addition, Trp398 might form inter-monomer interaction, e.g., with Arg287, linking α8 - α12 together. Any change along the dimer-dimer interface will affect the interaction of the KPF loop with the membrane interacting helices (pink in Supplemental Figure 9C). We suggest that even subtle reorientations of the α9 - α11 bundle with respect to the membrane plane might alter the geometry of membrane fission and could cause the phenotypical change in membrane morphology in EHD1^{R398W}.

Another hypothesis explaining the functional deficit of the R398W mutant is based on the seminal works of Daumke et al. [11, 12]. EHD1 and EHD4 (mouse EHD4 ADP conformation structure: pdb 5MVF; mouse EHD4 ATP conformation structure: pdb 5MTV) are well conserved at the protein level, and the published sequences of EHD2 (mouse EHD2 pdb 2QPT) and EHD4 are very similar, so we are confident the modeling is accurate. According to our modeling, the mutated R398 of human EHD1 lies very close to the nucleotide-binding pocket of an adjacent EHD1 protein within the EHD1 oligomer, based upon the crystal packing structure (Supplemental Figure 10). The conversion of R398 to W would result in a likely physical constraint of the loops constituting the nucleotide-binding pocket. This, we predict, would either interfere with nucleotide binding, nucleotide hydrolysis, or release of nucleotide following catalysis. We favor the last two based upon the cellular phenotype of the mutant, which is membrane-bound (suggesting binding to ATP), and able to drive membrane tubulation consistent with a lack of membrane fission (Supplemental Figure 11). This in fact is similar to the phenotype seen with ATPase-deficient mutant T94A in EHD2 [11] strongly arguing for this mechanism as at least a contributing mechanism.

Statistics

Data are shown in mean values ± standard error of the mean (SEM); “n” stands for the number of observations. Unpaired two-sided Student’s t-test and ANOVA with Tukey's or Dunnett's multiple comparison tests were used to calculate significance between different groups or time series, respectively. A p-value ≤ 0.05 was accepted to indicate statistical significance, which was identified by an asterisk (*). Statistics were performed using Origin V94E (OriginLab Corporation), SPPSS and GraphPad Prism software.

Supplemental Tables

Supplemental Table 1: Clinical phenotype details

Patient	Age at diagnosis [years]	Albumin / creatinine ratio [mg/g]	24-h urine protein [g]	β2M [mg/l]	Plasma Creatinine [mg/dl]	DMSA Renal uptake left / right [%]	Audiogram
1.1	11	189	2.1	121	0.5	2 / 1	SND
2.3	10	ND	1.0	42	0.6	6 / 6	SND
3.1	5	155	1.7	160	0.8	3 / 3	SND
3.2	12	ND	1.3	67	0.7	4 / 6	SND
3.3	33	54	0.9	77	0.7	ND	SND
4.1	14	178	0.7	150	0.6	3 / 3	SND
normal		< 30	< 0.15	< 1.8	0.2-1.0*	> 21 / > 21	

Shown are pertinent clinical and biochemical data. Note proteinuria, which is predominantly low-molecular weight, as indicated by the elevated β_2-microglobulin (β2M).

Note also the very low uptake of ^{99m}Tc-dimercaptosuccinic acid (DMSA) by the kidneys in the five tested affected individuals. Renal scintigraphy was performed four hours after administering 0.5mCi/kg of DMSA intravenously. The images were acquired using a double-head scintillation gamma camera equipped with a low-energy-high-resolution collimator (Infinia, General Electric, Haifa, Israel). Posterior planar images in the supine position were acquired with a 256x256 matrix and zoom=1 until 250,000 counts were detected. Single photon emission computed tomography (SPECT) images were acquired with a 64x64 matrix, zoom=1, 120 projections 3° apart with 15 second/projection. Renal uptake was calculated using the method detailed by Groshar et al. (Quantitation of Renal Uptake of Technetium-99m DMSA Using SPECT. J Nucl Med. 1989;30:246-250). Kidney volumes and radioactive concentration measurements were calculated using a customized computer program. For each kidney the injected dose (ID) per cc (%ID/cc) was measured and multiplied by the kidney volume for the calculation of the total kidney uptake. The patient uptake values were compared to uptake values in a normal population.

Moreover, all patients have sensorineural deafness (SND).

*The creatinine reference is age dependent: at the age of the youngest participant (5 years) it would be 0.2-0.5 mg/dl, and of the oldest (a female): 0.7-1.0 mg/dl. Note that plasma creatinine values are in the normal range for all. ND: not done.

Supplemental Table 2: Breeding statistics

n	female	male	*Ehd1*$^{+/+}$ pups	*Ehd1*$^{+/-}$ pups	*Ehd1*$^{-/-}$ pups	*Ehd1*$^{R398W/R398W}$ pups	*Ehd1*$^{R398W/wt}$ pups	*Ehd1*$^{wt/wt}$ pups	total
6*	*Ehd1*$^{+/–}$	*Ehd1*$^{+/–}$	60 (28%)	132 (61.7%)	22 (10.3%)				214
1	*Ehd1*$^{–/–}$	*Ehd1*$^{+/–}$	0	4 (80.0%)	1 (20%)				5
3	*Ehd1*$^{+/+}$	*Ehd1*$^{–/–}$	0	0	0				0
5*	*Ehd1*$^{R398W/wt}$	*Ehd1*$^{R398W/wt}$				32 (19.2%)	88 (52.7%)	47 (28.1%)	167
2*	*Ehd1*$^{R398W/wt}$	*Ehd1*$^{R398W/R398W}$				0	0	0	0

n denotes the number of breeding pairs; some breeding pairs produced multiple litters (*).

Ehd1$^{R398W/R398W}$: Knockin mice homozygous for the *Ehd1* mutation R398W.
Ehd1$^{R398W/wt}$*:* Knockin mice heterozygous for the *Ehd1* mutation R398W.
Ehd1$^{wt/wt}$*:* Littermates of knockin mice without the mutation R398W.
% was calculated for each genotype based on total genotyped pups for each breeding scheme.

Homozygous *Ehd1*$^{-/-}$ and *Ehd1*$^{R398W/R398W}$ male mice were bred for at least two months with at least one heterozygous or wildtype fertile female mouse. These breeding pairs produced no offspring indicating that male homozygous *Ehd1*$^{-/-}$ and *Ehd1*$^{R398W/R398W}$ mice were infertile.

Supplemental Figures

Supplemental Figure 1: EHD1 in human kidney

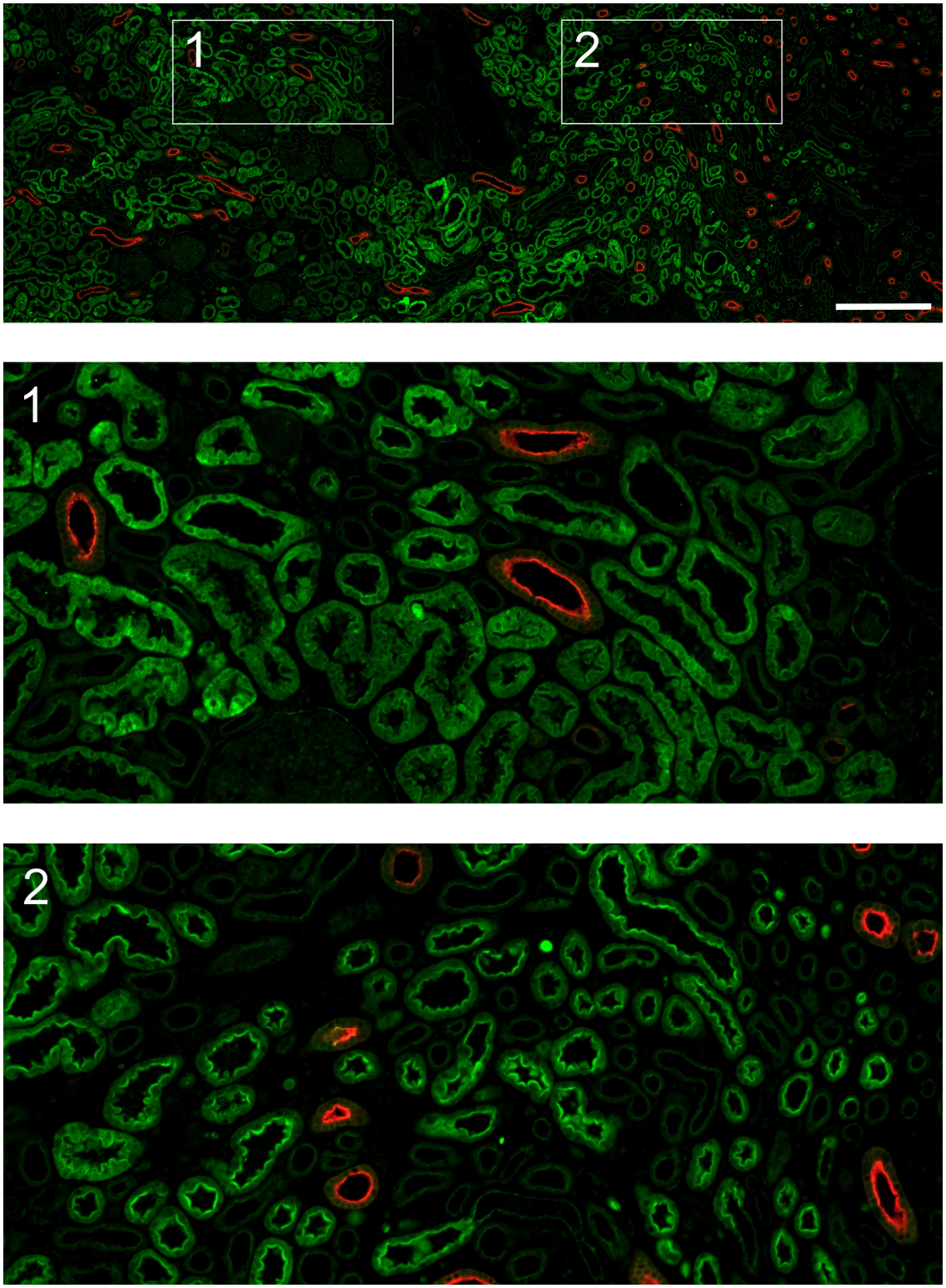

Localization of EHD1 (green) in normal human kidney. Aquaporin-2 is labeled in red. The middle panel and lower panel are magnifications of the areas marked in the upper panel. Strong EHD1-positive labeling was present in proximal tubules. Scale bar 500 µm.

Supplemental Figure 2: Ehd1 in mouse kidney

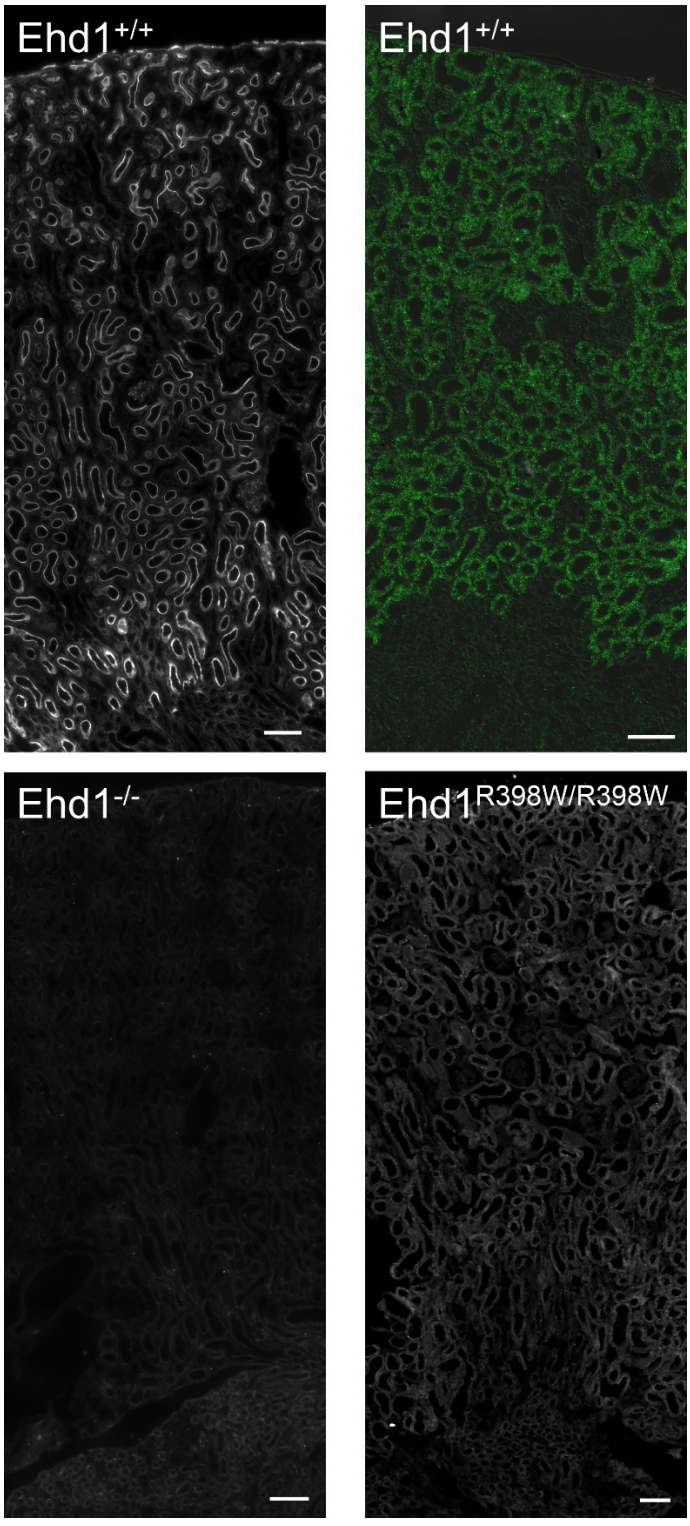

Similar to the localization in human kidney, Ehd1 was found in the apical/subapical compartment of proximal tubules using antibody staining (upper left panel) or RNAScope (upper right panel). In kidney cortex of a knockout mouse (lower left panel) no Ehd1-specific antibody staining was observed while knockin mouse showed limited granular staining (lower right panel). Scale bars 100 µm.

Supplemental Figure 3: Localization Ehd1, Megalin and reabsorbed β_2-microglobulin

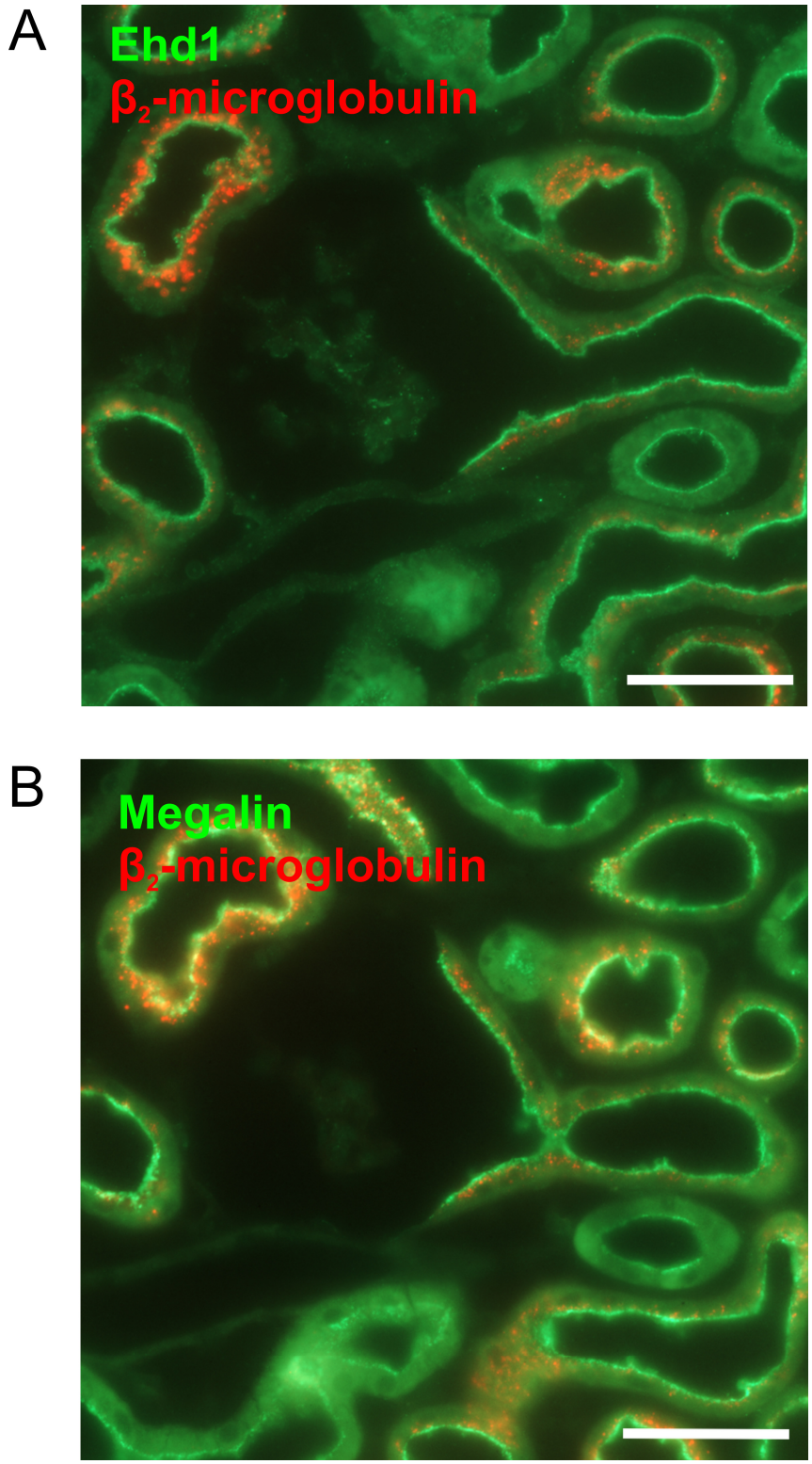

Ehd1 and Megalin show an overlapping subcellular localization. (A) Murine Ehd1 (green) was immunostained in the kidney of a mouse that was injected with labeled β_2-microglobulin (red) 30 min prior to fixation. Please note localization of β_2-microglobulin and Ehd1 in the apical/subapical compartment. (B) In a consecutive section (lower panel), Megalin (green) is also localized in the apical/subapical compartment. Scale bars: 50 µm.

Supplemental Figure 4. Zebrafish

A

	Hs EHD1	Dr Ehd1a	Dr Ehd1b	Dr Ehd2a	Dr Ehd2b	Dr Ehd3
Hs EHD1	100	85	87	61	68	88
Dr Ehd1a	85	100	89	61	68	83
Dr Ehd1b	87	89	100	61	70	85
Dr Ehd2a	61	61	61	100	73	62
Dr Ehd2b	68	68	70	73	100	70
Dr Ehd3	88	83	85	62	70	100

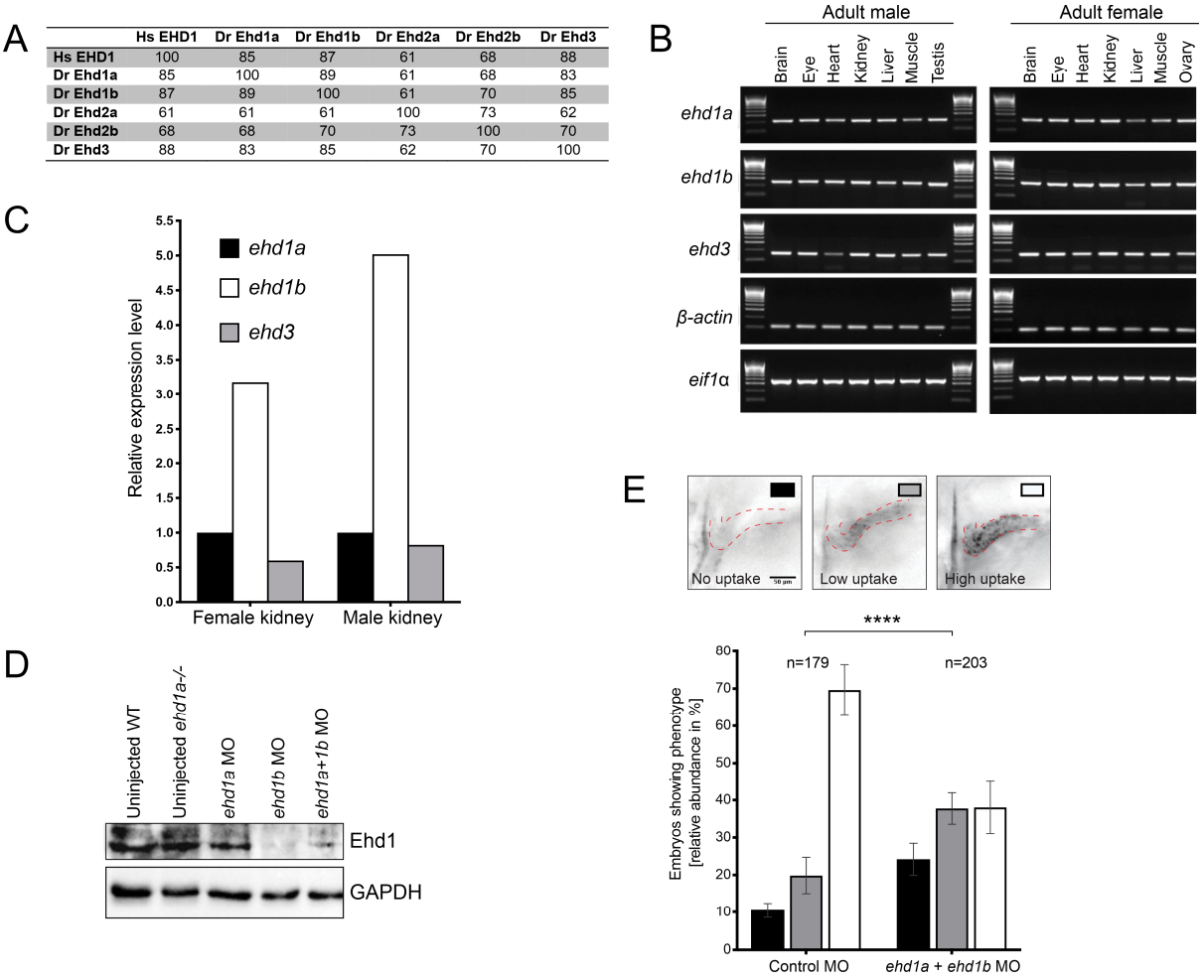

Expression analysis of zebrafish *ehd* orthologues and a role for Ehd1 in proximal tubular uptake. (A) Homology at the protein levels between human (Hs) EHD1 and the zebrafish (Dr) Ehd proteins. (B) RT-PCR analysis of tissue expression of zebrafish *ehd* transcripts. Shown is a representative PCR of tissue samples prepared from a total 18 animals, 3 biological replicates. (C) Q-PCR analysis of zebrafish *ehd1a*, *ehd1b* and *ehd3* expression in the adult zebrafish kidney. The Q-PCR was performed in duplicate, each time from samples prepared from 3 biological replicates. Values are normalized to the housekeeping gene *eif1a*. (D) Western blot of protein extracts from 3 dpf uninjected wildtype or *ehd1a*-null larvae or wildtype larvae injected with splice-blocking morpholinos to *ehd1a*, *ehd1b*, or both *ehd1a* and *ehd1b*. Ehd1a and b were detected with anti-EHD1 antibody. GAPDH is a loading control. Shown is a representative Western blot of samples prepared from approximately 100 larvae per condition. (E) Uptake of Alexa488-conjugated 10 kDa dextran into the pronephric tubules of 4 dpf zebrafish larvae treated with control morpholino (MO) or morpholinos targeting ehd1a and ehd1b. Uptake was assessed at 2.5 h post-injection by fluorescence stereomicroscopy and is scored as indicated. The bars correspond to the relative abundance of the different categorized phenotypes shown in the microscopy images (black, no uptake; grey, low uptake; white, high uptake). Data are presented as the mean ± SEM. Statistical analysis was performed using the Pearson's chi-squared test. **** indicates $p \leq 0.0001$.

Supplemental Figure 5: Localization of Ehd1^{R398W} in mouse kidney

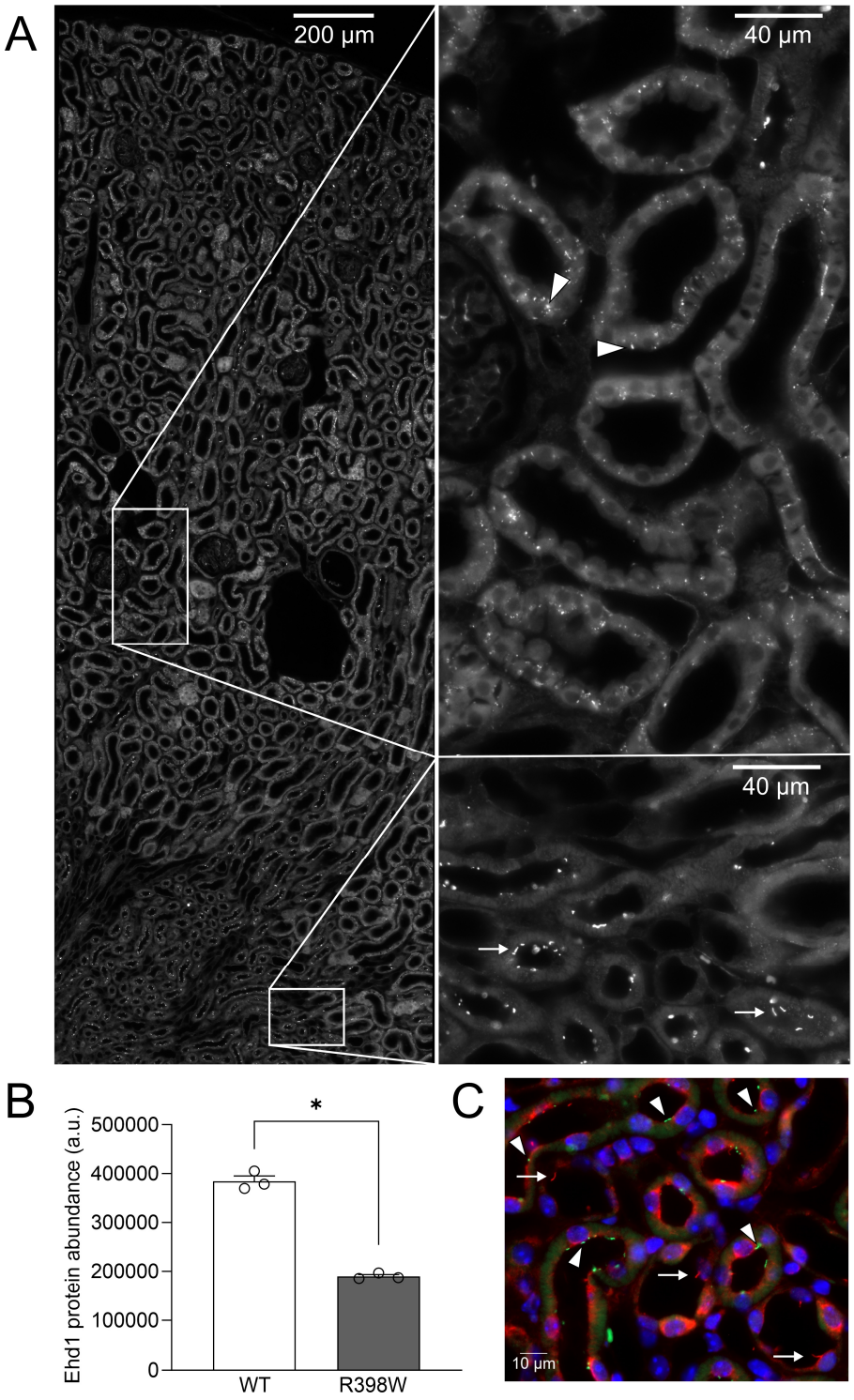

(A) In kidneys of homozygous *Ehd1*$^{R398W/R398W}$ knockin mice, Ehd1-specific immunostaining was sparse and mainly localized in small aggregates within the proximal tubular cells (arrowheads). In distal segments such as thick ascending limbs, filament-like structures were found at the apical side (arrows). These Ehd1-positive apical structures were absent in wildtype mice and negative for acetylated tubulin. (B) Protein abundance determined by mass spectrometry of kidney lysates of wildtype and *Ehd1*$^{R398W/R398W}$ mice revealed reduced Ehd1 protein abundance in knockin mice (n=3 each group). (C) No overlap between Ehd1-positive structures (green, arrowheads) and acetylated tubulin (red, arrows).

Supplemental Figure 6: Localization of Ehd1 and Arf6 in mouse kidneys

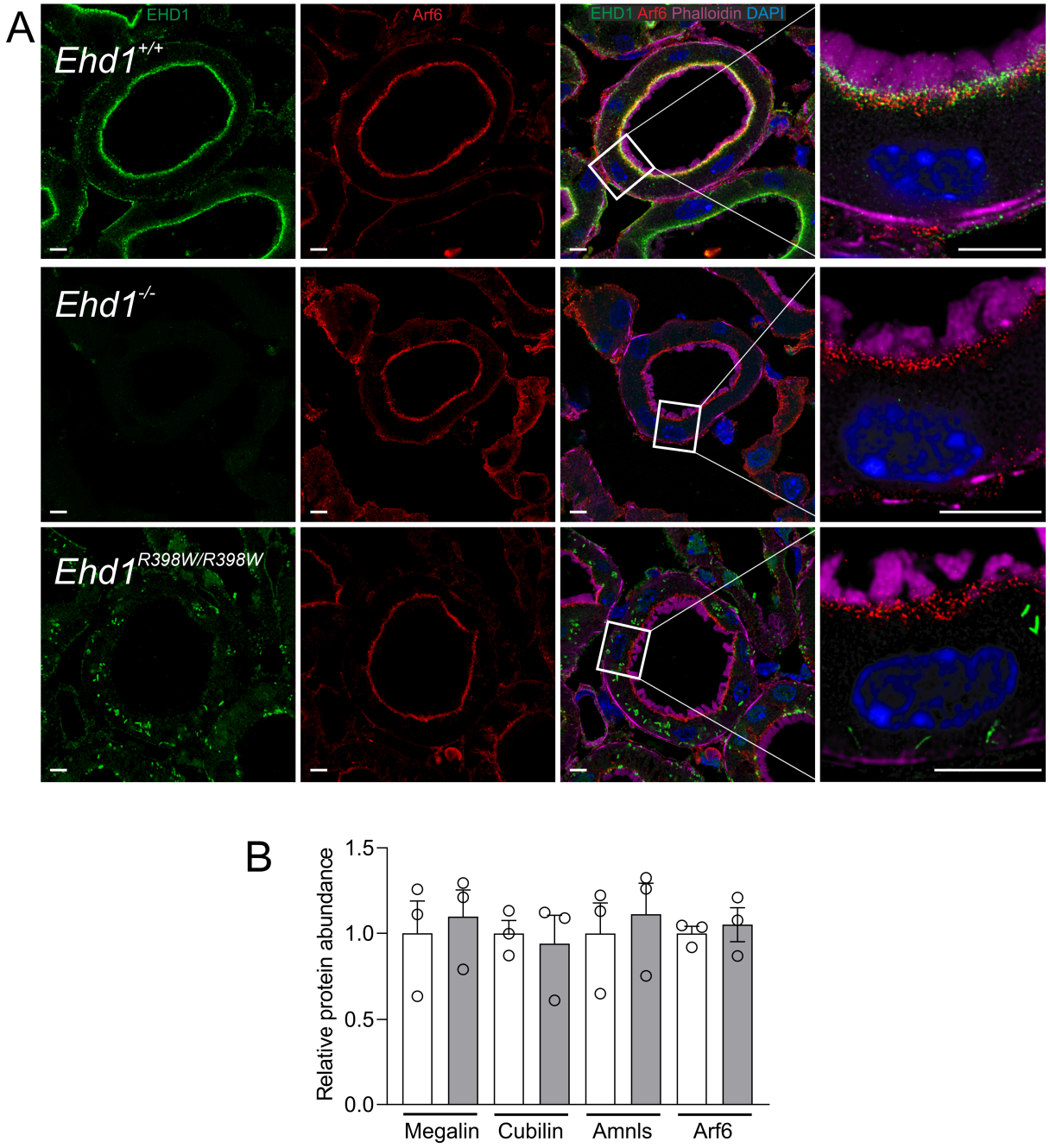

(A) Localization and abundance of Arf6 (red), a factor involved in trafficking of biological membranes and protein cargo, appeared to be similar in wildtype mouse kidney (upper panels), Ehd1 knockout (middle panels) and *Ehd1*$^{R398W/R398W}$ knockin mice (lower panel). Ehd1 (green); Phalloidin (magenta) was used as a marker of the brushborder membrane; nuclei were stained with DAPI (blue). Left three panels: confocal images; right panel: STED image for Ehd1 and Arf6. Deconvolution of all images using Huygens software. Scale bar: 5 µm. (B) Relative protein abundance of Megalin, Cubilin, Amnionless (Amnls), and Arf6, determined by mass spectrometry of kidney lysates of wildtype (white bars) and *Ehd1*$^{R398W/R398W}$ mice (gray bars). n=3 each group.

Supplemental Figure 7: Effect of *Ehd1* knockout and knockin on the localization of Rab11

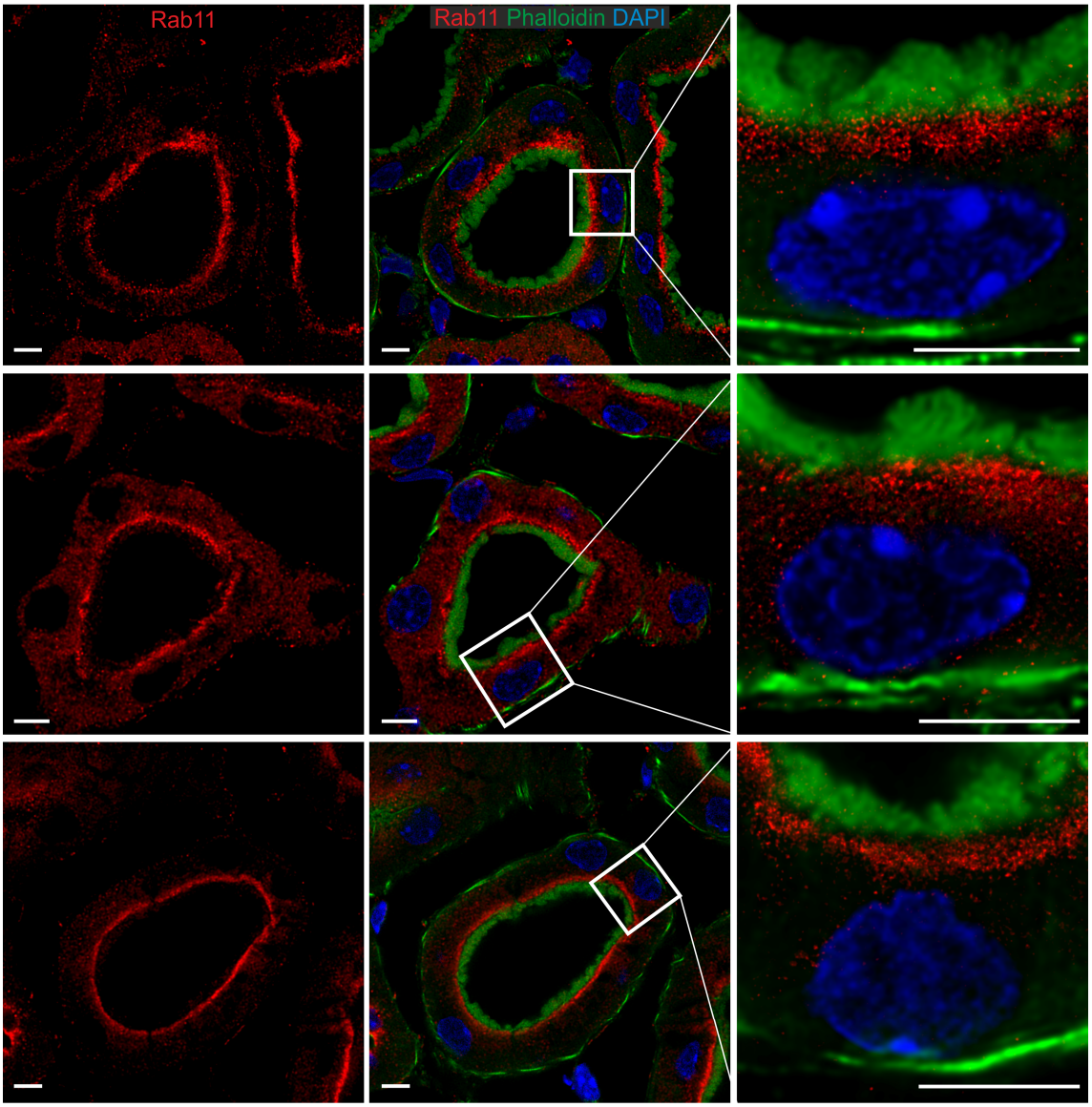

Localization and abundance of Rab11, a regulator of intracellular membrane trafficking routes, appeared to be similar in wildtype mouse kidney (upper panels), Ehd1 knockout (middle panels) and *Ehd1*$^{R398W/R398W}$ knockin mice (lower panel). Phalloidin (green) was used as a marker of the brushborder membrane; nuclei were stained with DAPI (blue). Left two panels: confocal images; right panel: STED image for Rab11. Deconvolution of all images using Huygens software. Scale bar: 5 µm

Supplemental Figure 8: Intravital multiphoton microscopy

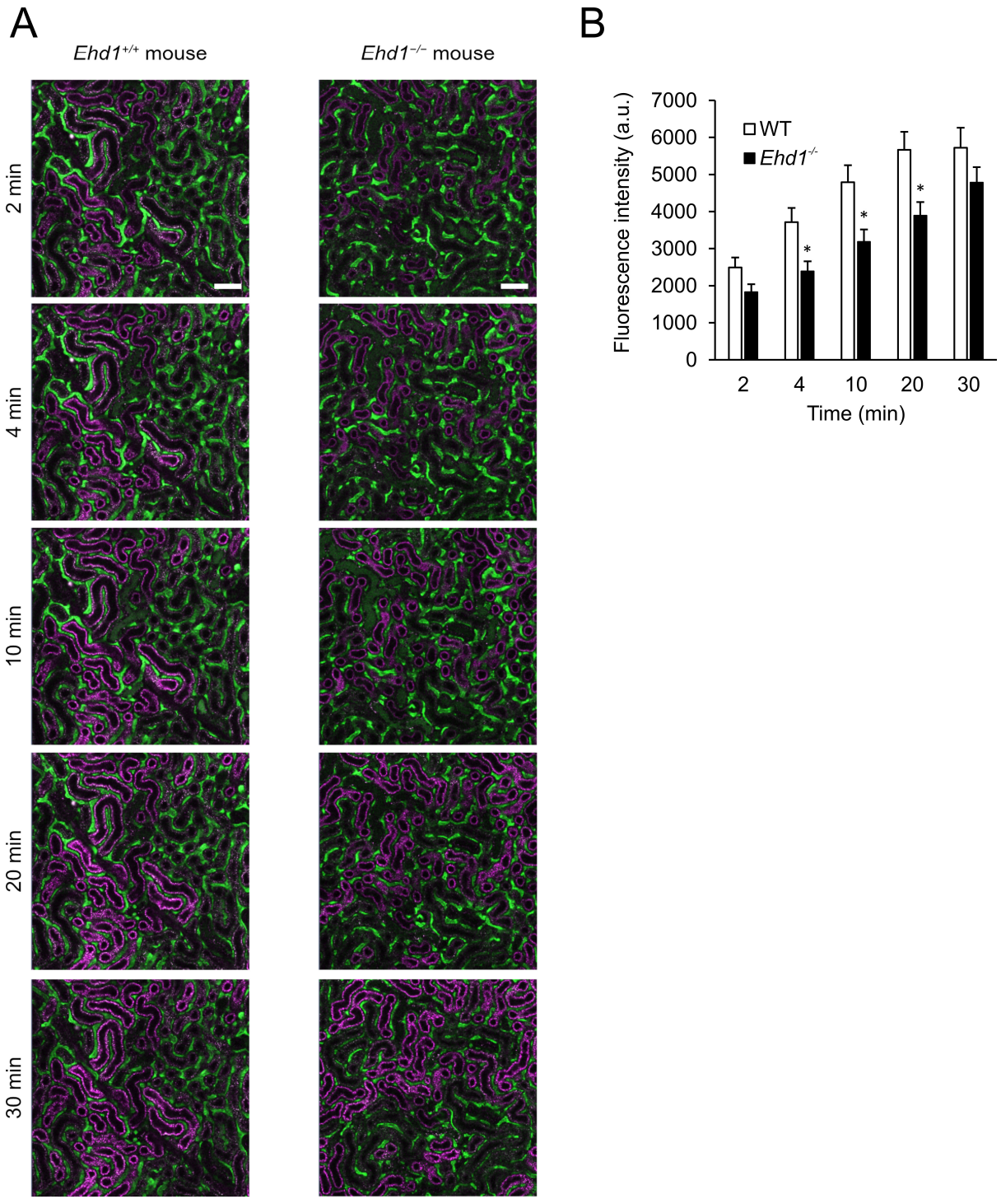

(A) Original intravital microscopy experiments illustrating the delayed reabsorption of labeled β_2-microglobulin (magenta) in the kidney of an Edh1$^{-/-}$ mouse. Blood vessel are stained by FITC-coupled high molecular dextran (green). Scale bars 75 µm. (B) Summary of experiments (6 animals each group, 31-36 tubules per group) as shown in (A) to illustrate the time course of the reduced rate of reabsorption. The data at 10 min are identical to the data shown in Figure 3G. Asterisks indicate $p \leq 0.05$.

Supplemental Figure 9: EHD1 and MICAL-L1 in EDH1-overexpressing LLC-PK1 cells

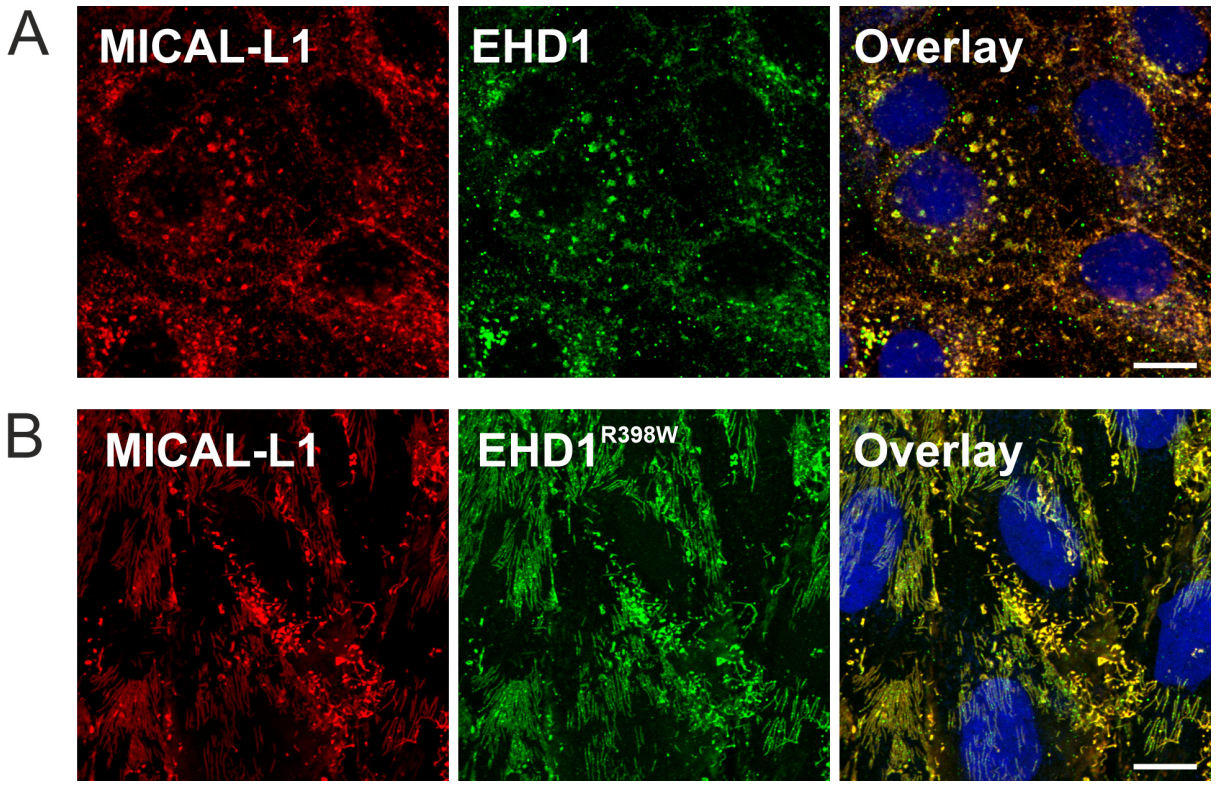

Immunofluorescence microscopy of LLC-PK1 cells expressing wildtype human EHD1 (A) or the EHD1^{R398W} mutant (B). MICAL-L1 (red) colocalized with EHD1 (green) in cells expressing wildtype and mutant EHD1. In the overlay images, cell nuclei were stained with DAPI (blue). Cells were induced for 48 h with doxycycline (1 mg/l). Scale bar: 10 µm.

Supplemental Figure 10: MICAL-L1 and Pacsin 2 in cells overexpressing EDH1^{R398W}

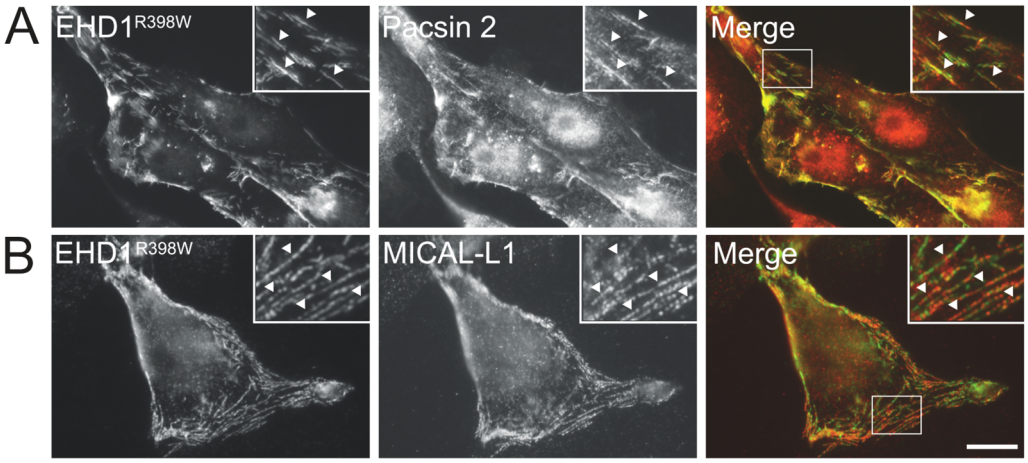

Immunofluorescence microscopy of LLC-PK1 cells expressing the EHDR398W mutant, labelled with antibodies to EHD1 and either Pacsin 2 (A) or MICAL-L1 (B) to label recycling endosomes. In the overlay images, EHD1 is shown in green, Pacsin 2 and MICAL-L1 in red. Arrowheads indicate colocalization within tubules. Cells were induced for 24 h with doxycycline. Scale bar: 20 µm.

Supplemental Figure 11: Primary cilia in murine and human kidneys

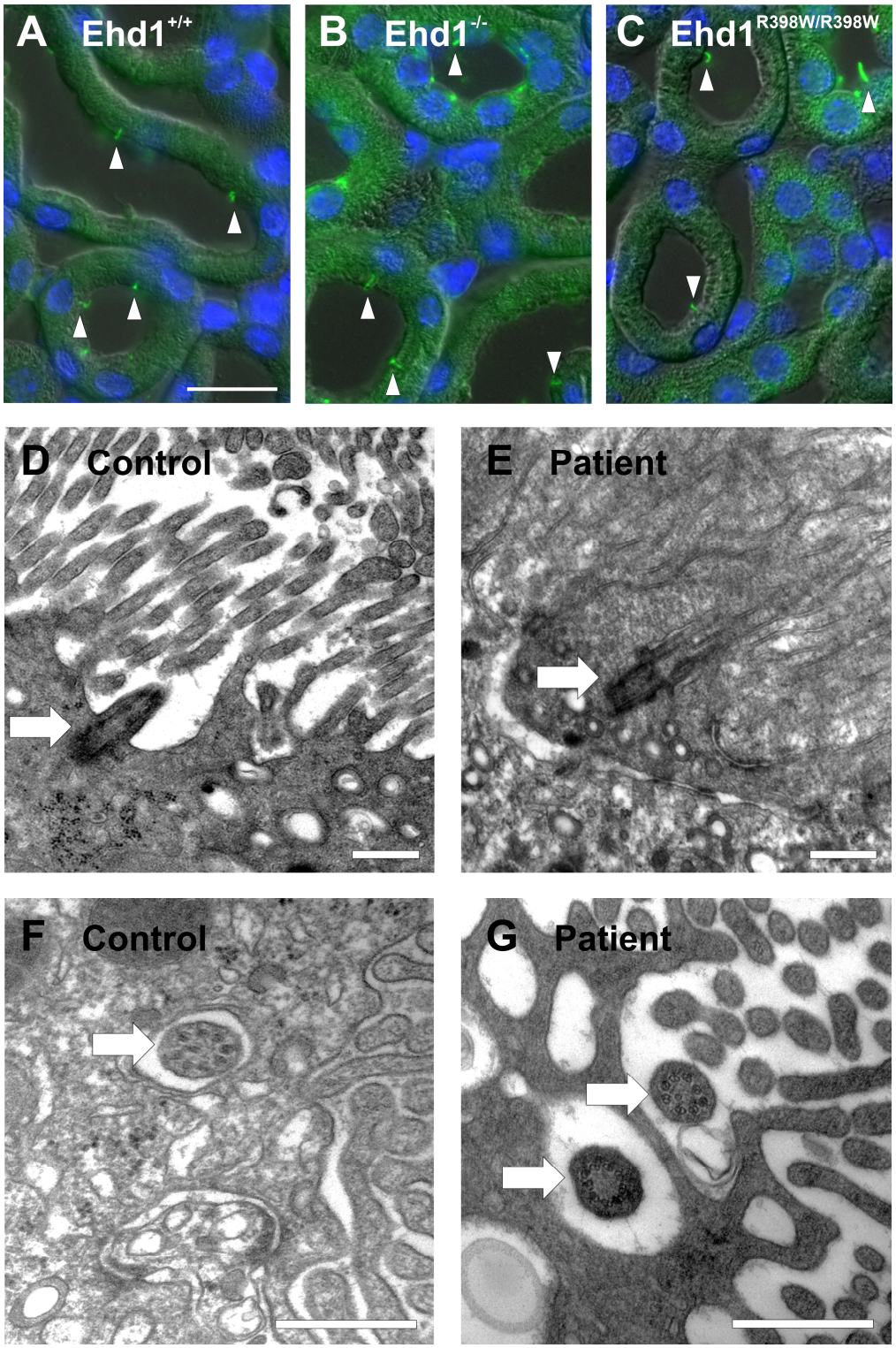

Proximal tubules of wildtype (A), homozygous Ehd1 knockout (B), and R398W knockin mice (C) had similar numbers of Arl13b-positive primary cilia (arrow heads). Scale Bar 20 µm. Electron microscopy (EM) of primary cilia (arrows) within human renal proximal tubules. EM normal kidney (D) / (F); EM affected individual (E) / (G). Please note, (D) and (E) show the base of cilia (longitudinal slice); (F) and (G) show a cross section of cilia. Scale Bars 500 nm.

Supplemental Figure 12: Alignment of EHD1, EHD2 and EHD4

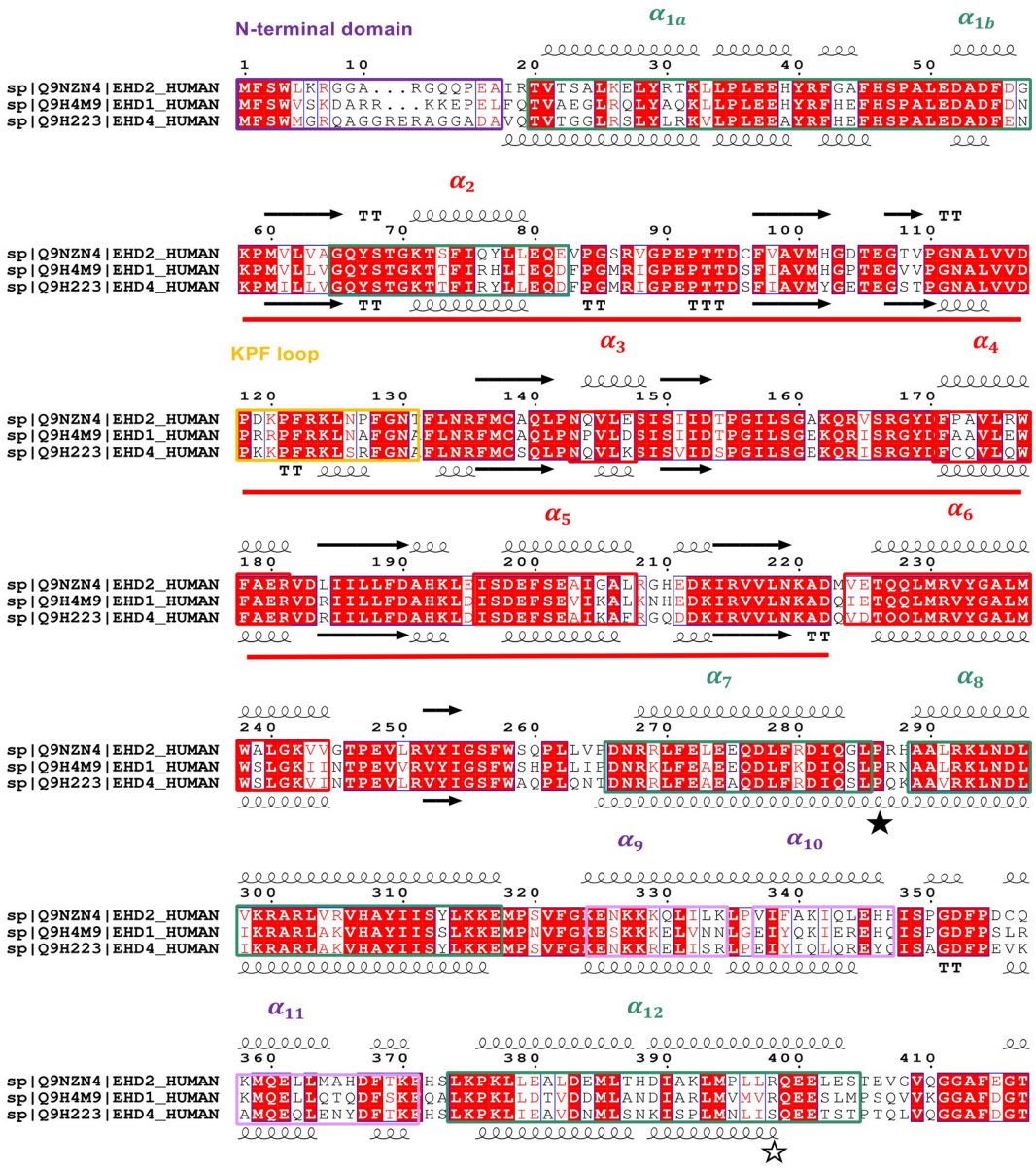

Multisequence alignment of human EHD1 (Q9H4M9), EHD2 (Q9NZN4) and EHD4 (Q9H223) by the program Clustal Omega reveals an overall identity between these isoforms of > 70%. The topology based on crystal structures of EHD2 (pdb entry code 4CDI) and EHD4 (pdb entry code 5MTV) is shown on top and bottom of the respective sequences. EHD proteins consist of an N-terminal unordered domain (purple), a small helical domain α1(dark cyan), the GTPase domain comprising α2 - α5 (red), several β-sheets (indicated as black arrows) and the dimerization interface helix α6. Adjacent to the GTPase domain is the helix pair α7 - α8 (dark cyan) separated by the hinge residue Pro286 (black star) and the membrane interacting helices α9 - α11(pink). Helix α12 connects to the EH-domain (not shown) via a long unordered linker loop. The mutation Arg398Trp in EHD1 is located at the very end of α12 (white star).

Supplemental Figure 13: Structural modeling: Putative structure of EHD1 dimers

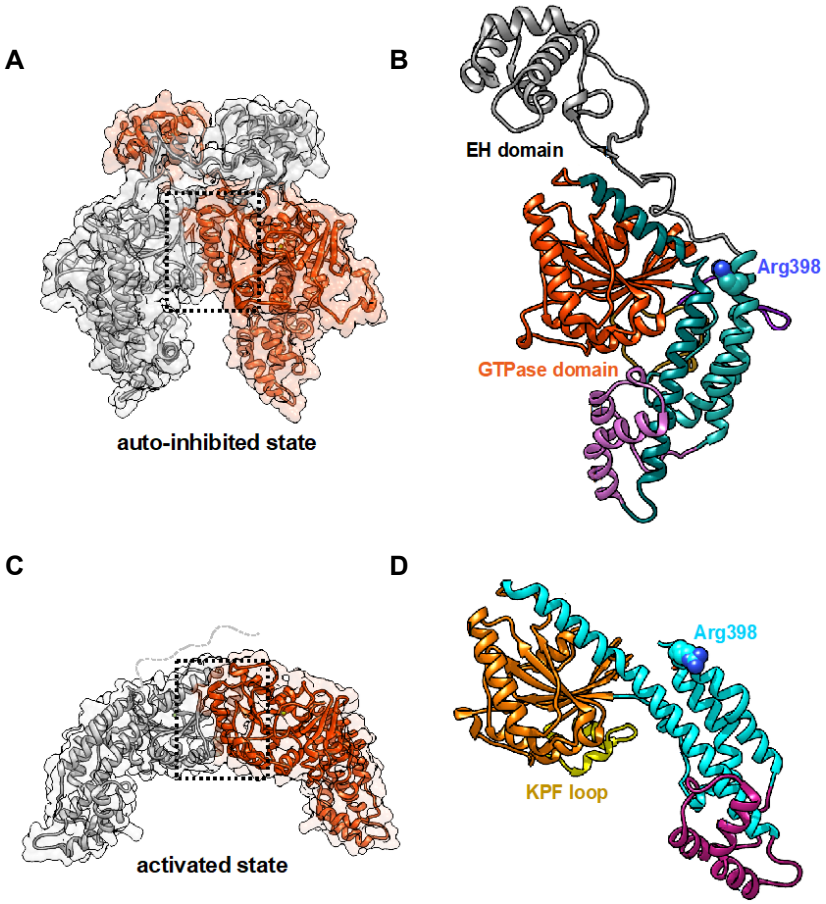

Homology models of EHD1 determined by the program Modeller using the autoinhibited state of EHD2 (pdb entry code 4CDI) (A and B) and the activated state of EHD4 (pdb entry code 5MTV) (C and D) as a template, respectively. A and C: Similar to EHD2 and EHD4, EHD1 presumably forms stable dimers (monomers are colored in red and grey) with α6 serving as dimerization helix (box in dotted line). EH-domains are only resolved in the auto-inhibited state locking the ATPase domain of the neighboring monomer in the dimer. Although the EH-domain of EHD4 was present during crystallization it was not resolved suggesting that the blocking interaction was released during activation. Since EH domains were not resolved in the activated state, they are not shown in (C) and (D). The higher degree of flexibility is in agreement with the functional role of EH-domain as interaction partners for different proteins in the activated state. The domain structure in the EHD1 homology model is shown in the putative autoinhibited state (B) and the activated state (D). Arg398 is shown in sphere representation located at the end of α12. The KPF loop is only ordered in the activated state (colored in gold in (D)).

Supplemental Figure 14: Structural modeling: Effects of the R398W mutation on EHD1 oligomerization

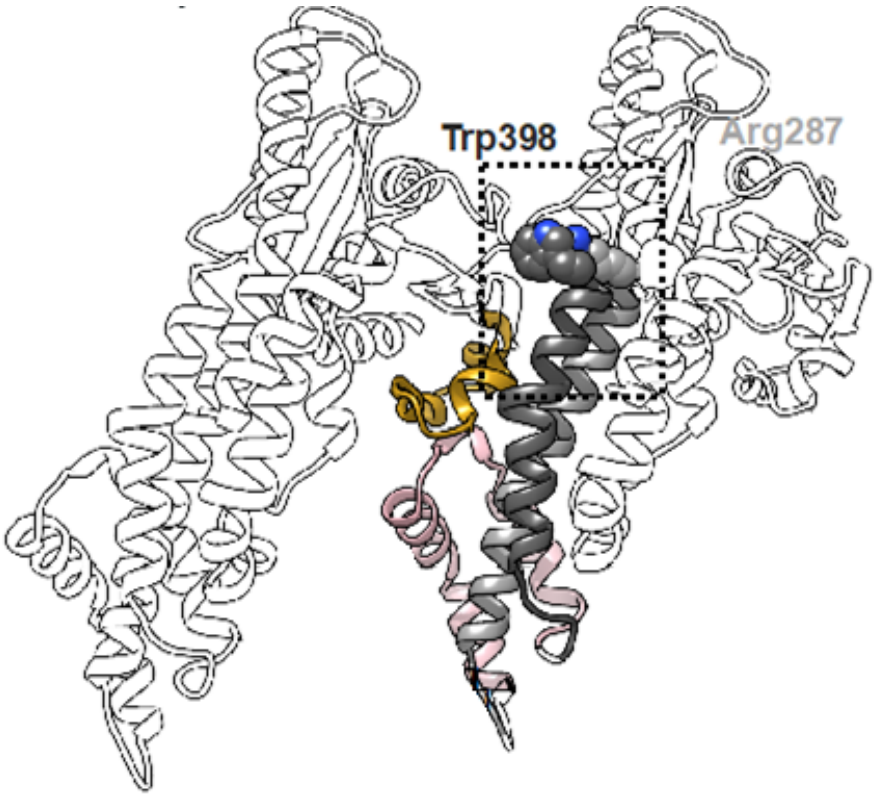

Mutation of Arg398 against a bulky residue such as tryptophan probably disturbs the dimer-dimer interaction between the KPF loop and the helical bundle and thereby prevents oligomerization. A possible pathological interaction partner of Trp398 suggested from homology modelling would be Arg287, which would strengthen the interactions between $\alpha_{12}$and α_8 within one monomer.

Supplemental References

1. Cebrian-Serrano A, Zha S, Hanssen L, Biggs D, Preece C, Davies B: Maternal Supply of Cas9 to Zygotes Facilitates the Efficient Generation of Site-Specific Mutant Mouse Models. PLoS One 12**:** e0169887, 2017 doi: 10.1371/journal.pone.0169887
2. Theilig F, Kriz W, Jerichow T, Schrade P, Hahnel B, Willnow T, et al.: Abrogation of protein uptake through megalin-deficient proximal tubules does not safeguard against tubulointerstitial injury. J Am Soc Nephrol 18**:** 1824-1834, 2007
3. Marshansky V, Bourgoin S, Londono I, Bendayan M, Vinay P: Identification of ADP-ribosylation factor-6 in brush-border membrane and early endosomes of human kidney proximal tubules. Electrophoresis 18**:** 538-547, 1997
4. Schilling A, Gerum R, Krauss P, Metzner C, Tziridis K, Schulze H: Objective Estimation of Sensory Thresholds Based on Neurophysiological Parameters. Front Neurosci 13**:** 481, 2019 doi: 10.3389/fnins.2019.00481
5. Lu Q, Insinna C, Ott C, Stauffer J, Pintado PA, Rahajeng J, et al.: Early steps in primary cilium assembly require EHD1/EHD3-dependent ciliary vesicle formation. Nat Cell Biol 17**:** 228-240, 2015 doi: 10.1038/ncb3109
6. Oltrabella F, Pietka G, Ramirez IB, Mironov A, Starborg T, Drummond IA, et al.: The Lowe syndrome protein OCRL1 is required for endocytosis in the zebrafish pronephric tubule. PLoS Genet 11**:** e1005058, 2015 doi: 10.1371/journal.pgen.1005058
7. Fischer R, Kessler BM: Gel-aided sample preparation (GASP)--a simplified method for gel-assisted proteomic sample generation from protein extracts and intact cells. Proteomics 15**:** 1224-1229, 2015 doi: 10.1002/pmic.201400436
8. Reinders J, Altenbuchinger M, Limm K, Schwarzfischer P, Scheidt T, Strasser L, et al.: Platform independent protein-based cell-of-origin subtyping of diffuse large B-cell lymphoma in formalin-fixed paraffin-embedded tissue. Sci Rep 10**:** 7876, 2020 doi: 10.1038/s41598-020-64212-z
9. Gillet LC, Navarro P, Tate S, Rost H, Selevsek N, Reiter L, et al.: Targeted data extraction of the MS/MS spectra generated by data-independent acquisition: a new concept for consistent and accurate proteome analysis. Mol Cell Proteomics 11**:** O111 016717, 2012 doi: 10.1074/mcp.O111.016717
10. Simburger JMB, Dettmer K, Oefner PJ, Reinders J: Optimizing the SWATH-MS-workflow for label-free proteomics. J Proteomics 145**:** 137-140, 2016 doi: 10.1016/j.jprot.2016.04.021
11. Daumke O, Lundmark R, Vallis Y, Martens S, Butler PJ, McMahon HT: Architectural and mechanistic insights into an EHD ATPase involved in membrane remodelling. Nature 449**:** 923-927, 2007 doi: 10.1038/nature06173
12. Melo AA, Hegde BG, Shah C, Larsson E, Isas JM, Kunz S, et al.: Structural insights into the activation mechanism of dynamin-like EHD ATPases. Proc Natl Acad Sci U S A 114**:** 5629-5634, 2017 doi: 10.1073/pnas.1614075114